JOURNAL OF SPACECRAFT AND ROCKETS
Vol. 46, No. 5, September–October 2009

Plasma Actuation for the Control of a Supersonic Projectile

Patrick Gnemmi* and Christian Rey†
French–German Research Institute of Saint-Louis, F-68301 Saint-Louis Cedex, France

DOI: 10.2514/1.40792

The generation of a plasma discharge on a projectile surface seems to be a way of producing a pressure imbalance to divert a projectile from its initial trajectory. Thus, some experiments dealing with the steering of a supersonic projectile by using a plasma actuator are presented. The plasma discharge is produced by an embedded low-voltage generator capable of delivering an electric discharge between the electrodes flush with the projectile surface. A first series of experiments carried out under wind-tunnel conditions at a Mach number of 3 allows the detailed study of the perturbation evolution along the projectile surface, the disturbance being generated by the plasma discharge. A second series of experiments in the wind tunnel at the same Mach number demonstrates that a plasma discharge generates the angular deviation of a fin-stabilized projectile: 243 J of stored energy delivered in 2.5 ms at the cone–cylinder junction of the projectile induces an angle of attack of 2 deg after the plasma-discharge generation. Other experiments conducted in a shock-tube facility under low-altitude conditions prove that it is possible to activate a plasma discharge on a projectile flying at a Mach number of 6.

I. Introduction

THE change in the trajectory of a flying vehicle is made possible by unbalancing the pressures exerted on the body surface. This pressure imbalance can be produced by the deployment of control surfaces [1–9] or by the use of one or more pyrotechnical mechanisms judiciously distributed along the vehicle [10–15]. In the case of supersonic projectiles, the major drawback to the use of the surface-spreading technique is that large forces are involved for the deployment of surfaces to overcome the very high pressures encountered at high velocities. Thus, the use of pyrotechnical mechanisms is more appropriate for high-speed vehicles, but the fact that the pyrotechnical mechanism works only once and produces everything or nothing is a main drawback when a controlled angle of attack must be given.

The idea of generating electric discharges producing a plasma on the projectile surface comes from the analysis of different solutions for steering a guided supersonic projectile (GSP) flying at a Mach number (M) ranging from 3 to 4 [16]. The GSP is a short-range guided antiaerial projectile launched by a 40 mm gun and designed to increase its precision when faced with increasingly agile aerial vehicles flying up to a few kilometers of altitude. The underlying idea consists of giving the GSP a maneuvering capacity, allowing it to compensate for the trajectory prediction error. The plasma-actuator steering concept consists of unbalancing the flow around the projectile nose by producing one or several plasma discharges near the projectile nose. A patent describing the concept and a first high-voltage system was registered in February 2002 and was issued in France in January 2005 and in the United States in February 2006 [17]. A new low-voltage device was designed to avoid the high-voltage apparatus drawbacks and a patent was also registered in September 2005, was issued in France in December 2007, and was published in the United States in August 2007 [18].

Flow control around aerial vehicles using plasma has been part of the fluid dynamics flow control community for more than a decade. The most recent state of the art concerning a type of plasma actuator is given in [19]. That plasma actuator that is being used widely is based on a dielectric barrier discharge mechanism that has desirable features for use in air at atmospheric pressures. It has been employed in a wide range of applications that include drag reduction at supersonic speeds [20–22], steering vehicles at supersonic speeds [23], exciting boundary-layer instabilities at supersonic speeds [24–27], lift increase on a wing section [28–31], low-pressure turbine-blade separation control [32–37], turbine tip-clearance flow control [38,39], bluff-body flow control [40–42], turbulent boundary-layer control [43,44], unsteady vortex generation and control [45,46], and airfoil-leading-edge separation control [47–50].

Analysis of the previous publications shows that few studies are being conducted on supersonic projectile steering by the use of a plasma discharge. Therefore, the work described in this paper is original; indeed, a plasma-discharge production on the surface of a supersonic projectile flying in the low atmosphere has not been applied up until now for the control of projectiles in terms of a trajectory change.

Section II of the present paper deals with the principle of the concept for controlling a supersonic projectile by a plasma discharge. Section III describes in detail two plasma-discharge actuators. Section IV presents the experimental setups and the instrumentation used for the experiments. Section V shows the experimental results obtained in the wind-tunnel facility at Mach 3 and in the shock-tube facility at Mach 6. Section VI concludes the paper and proposes future investigations.

II. Principle of the Concept

In the case of a high-speed vehicle, a shock wave occurs at its nose tip or ahead of it, depending on the nose geometry. When the vehicle flies without any angle of attack, the pressures distributed on its surface balance one another out and the shock wave has symmetries depending on the vehicle geometry. For example, for a supersonic projectile forebody with a conical nose, the shock wave is attached to the cone tip and has itself a conical shape. The proposed concept consists of obtaining the asymmetry of the flow variables around the projectile nose by generating one or several plasma discharges at the nose tip to give an angle of attack to the projectile. Indeed, a single plasma discharge can produce an initial angle of attack followed by a damping motion, whereas a set of plasma discharges or a longer plasma discharge with constant power can produce a constant angle of attack.

Some theoretical investigations illustrate the feasibility of such a system [51]. Figure 1 presents the qualitative result of a numerical computation of the projectile forebody, flying from right to left near

Presented as Paper 6885 at the AIAA Atmospheric Flight Mechanics Conference, Honolulu, HI, 18–21 August 2008; received 4 September 2008; revision received 21 July 2009; accepted for publication 22 July 2009.

*Senior Scientist, Aerothermodynamics and Shock-Tube Department; patrick.gnemmi@isl.eu. Senior Member AIAA.

†Engineer, Aerodynamics and External Ballistics Department; christian.rey@isl.eu.

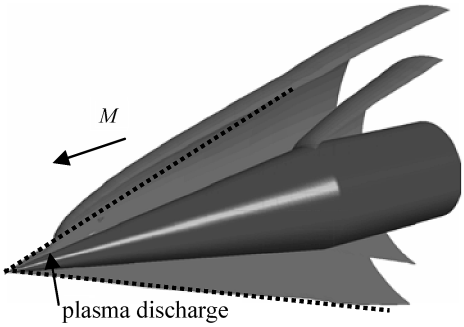

Fig. 1 Surfaces of constant pressure in the supersonic projectile flowfield undergoing a plasma discharge.

the ground level at a Mach number of 3.2. A plasma discharge modeled as a transverse hot jet is applied near the nose tip for a certain length of time. The figure shows the forebody and the halves of two surfaces. The surfaces represent a constant pressure in the flowfield, highlighting the main structure of the flowfield. The attached shock wave is perfectly visible at the tip of the conical nose as well as the Prandtl–Meyer expansion wave at the junction of the conical nose and the cylindrical part of the forebody. On the side of the conical nose where the plasma discharge is activated, the geometry of the shock wave is clearly distorted due to the generation of the plasma discharge. On the contrary, on the opposite side the geometry of the shock wave remains unperturbed.

The objective consists of generating one or several plasma discharges so that the asymmetry is large and long enough to cause the deviation of the projectile with respect to its initial trajectory. The absence of mobile parts and the repetitive effect of discharges are the main advantages of this technique. In fact, control of the vehicle could be achieved by repetitive discharges activated on demand, depending on the required trajectory.

III. Plasma-Discharge Actuators

A. Previous High-Voltage Generator

Within the framework of the feasibility study of the projectile control by plasma discharge [17,18,51], the interaction between a plasma discharge and the crossflow of a supersonic projectile was highlighted. That demonstration was performed in the course of experiments at supersonic speed during which a plasma discharge was generated at the tip of a projectile cone equipped with a high-voltage generator. The experimental conditions simulated a projectile flying at an altitude of about 5 km, at a Mach number of 4.56, and at angles of attack ranging from -5 to $+5$ deg. Visualizations performed using a differential interferometer (DI) (see Sec. IV.E) allowed the observation of the structure modification of the projectile flowfield due to the plasma-discharge effect. That change in structure causes the imbalance of the flowfield near the projectile and should allow its steering to be controlled. The plasma discharge was obtained by a high-voltage generator delivering an energy of 0.1 J under 20 kV; this generator is based on a high-voltage supply associated with a Marx generator. The use of such a generator allows the production of a very short discharge of about 1 μs; consequently, the effect on the flow is as short. Therefore, to obtain a significant effect it is necessary to increase that duration.

There are three possibilities of doing that: multiplying the number of very short discharges, increasing the duration of the plasma discharge, or combining these two alternatives. The increase in the plasma-discharge number allows the perturbation duration to be lengthened, as can be seen from the interferogram (see Sec. IV.E) in Fig. 2. The flow is traveling from left to right and the attached shock wave due to the supersonic speed of the flow is emphasized. Two perturbations due to the effect of two successive plasma discharges separated by 6.5 μs are visualized. Each plasma discharge has a duration of about 1 μs, and the total disturbance time is about twice that of the disturbance of a single plasma discharge, the amplitude of each discharge remaining the same. It is thus possible to multiply by

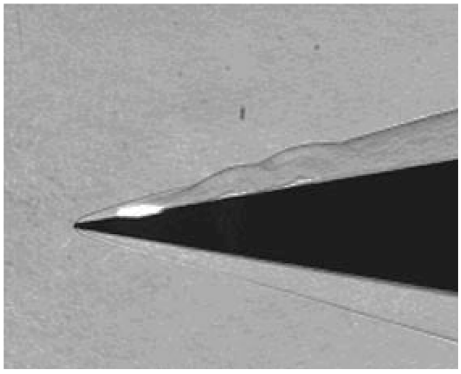

Fig. 2 Disturbances visualized by an interferogram recorded 19 μs after the first of a series of two plasma discharges separated by a duration of 6.5 μs.

N the disturbance duration by means of a system of N impulses judiciously separated from one another.

However, this way of operating has significant drawbacks. On the one hand, this system does not allow an easy increase in the disturbance amplitude; on the other hand, generating N impulses involves as a consequence the use of high-voltage generators, leading to an extremely bulky system that cannot be integrated into a mean-caliber projectile (projectile diameter: ≤ 50 mm).

B. New Low-Voltage Actuator

The low-voltage device is designed to avoid the drawbacks of the high-voltage one [18–52]. The choice of low voltage allows the use of more important capacitors, the increase in the available energy for a given volume, the avoidance of the constraints linked to the use and storage of the high voltage, and the reduction of the device dimensions, so that it can be embedded in a mean-caliber projectile.

The problem encountered for a low-voltage system is the following one: a low voltage (<1000 V) is not sufficient to disrupt the electric barrier existing between two electrodes a few millimeters from each other, even in a rarefied atmosphere. The Paschen curve gives the breakdown voltage in air at 293 K as a function of the product of the pressure with the distance between the electrodes [53] (electrode distance). In the present application, the projectile has to be steered at an altitude lower than a few kilometers, at which the pressure ranges from 10^5 to about 10^4 Pa. As an example and taking into account the Paschen curve, for an electrode distance of 5 mm and for a pressure of 10^4 Pa, it is necessary to apply a voltage higher than 3000 V to break the electric barrier. During supersonic flight, the pressure on a projectile forebody, where the electrodes are flush with the surface, is higher than the atmospheric pressure (depending on the projectile velocity); consequently, the breakdown voltage also has to be higher. The proposed device is composed of a high-voltage low-energy activation system and a low-voltage high-energy plasma generator that is able to produce a plasma discharge between two electrodes.

Let us consider a projectile flying from right to left and composed of a conical forebody equipped with two pairs of electrodes, as represented in step 1 of Fig. 3. The role of the high-voltage activation system only consists of breaking the electric barrier between two electrodes, then of ionizing a small gas volume (step 2). As the projectile flies, the ionized gas volume moves along its surface (steps 3 and 4). The ionized gas volume, which has a low impedance, activates a plasma discharge when it encounters two other electrodes supplied by a low voltage (step 5). The role of that low-voltage plasma generator consists of delivering the energy to the electrode pair and then producing the plasma discharge. It is obvious that the high-voltage activation-system electrodes have to be ahead of the electrodes of the low-voltage plasma generator.

The high-voltage activating system is composed of a low-voltage supply transmitting little energy to the ionizing supply and to the impulse generator. The ionizing supply and the impulse generator are connected to a step-up transformer generating the high voltage.

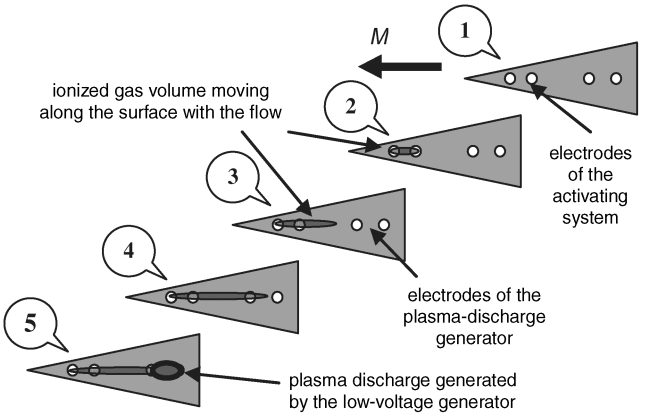

Fig. 3 Principle of the activation of a low-voltage plasma-discharge actuator.

The transformer is itself connected to the electrode pair. An external signal allows the triggering of the activation system. The transformer is the main part of the activation system. In the experiments presented in this paper, a 320 V/5000 V transformer was used; however, the plasma-actuator design could be adapted to any projectile-flight conditions.

The low-voltage plasma-discharge generator is composed of a capacitor connected to the electrode pair. The capacitor is charged by a low-voltage supply. Aluminum electrolytic capacitors meet the requirements for the present application; indeed, they have a large capacity/volume ratio and a low equivalent series resistance, allowing the use of a large discharge current. As an example, a capacitor with a 35 mm diameter and a 50 mm length supplied by 550 V has a stored energy of 50 J, which is 500 times higher than the one stored in the high-voltage plasma generator described in Sec. III.A.

In Fig. 4a, the plasma actuator embedded in a 50-mm-diam test model is shown. The low-voltage supply, used for charging the capacitor before the test is performed, is not embedded in the test model; an autonomous low-voltage supply based on a 3.2 V battery and a step-up transformer is being studied so that it can be embedded in the same test model. Figure 4b shows a close-up of the test model tip, thus displaying the electrodes; the cathode of the activation system and that of the low-voltage plasma generator have been brought together, limiting the number of electrodes to three. The brass cone tip, which is the anode of the activation system, is fixed to an electrically insulating part. The common cathode and the anode of the low-voltage plasma generator are mounted on that intermediate part. The steel part ensures the mechanical link between the first two parts and the cylindrical part of the test model.

IV. Experimental Setup and Instrumentation

A. Wind-Tunnel Facility

Some experiments are conducted in the 0.2×0.2 m^2 supersonic wind tunnel [11,54] at the French–German Research Institute of Saint-Louis (ISL) at $M = 3$. This facility operates in the blowdown mode with a blow duration of typically 50 s. The model-related Reynolds number based on the body diameter is 10^6; in the experiments reported in the present paper the static freestream pressure is $P_\infty = 0.1906 \times 10^5$ Pa and the static freestream temperature is 108 K.

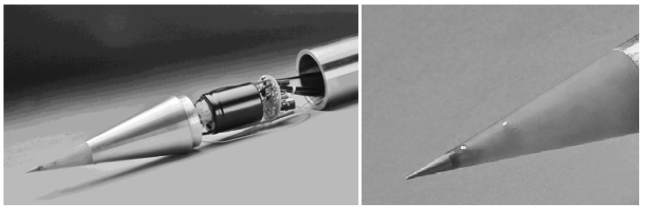

Fig. 4 Shown are the following: a) embedded low-voltage plasma-discharge actuator in a 50-mm-diam test model, and b) close-up of the electrodes.

B. Shock-Tube Facility

Other experiments are carried out at $M = 4.5$ and 6 in a shock tunnel [55–58] at ISL, in which the exact atmospheric flight conditions can be duplicated, ranging from ground level up to more than 30 km of altitude. The gas is expanded and accelerated inside the nozzle in such a way that the required real-flight conditions are present at the nozzle exit for 3–4 ms. The body is fixed inside the test chamber at the front of the nozzle and the airflow is accelerated up to the desired pressure, temperature, and flight velocity.

C. Fixed-Model Device

A series of experiments is performed with a model fixed in the wind tunnel and in the shock tube to mainly visualize and analyze the flowfield disturbed by the plasma discharge. The experimental study is conducted for the 50 mm test model of Fig. 4, which is mounted without any angle of attack on a shaft assembly along the wind-tunnel or shock-tube centerline. The electrodes flush with the conical surface are located at the model tip and are arranged along the longitudinal axis of the model, allowing the production of a geometrically quasi-linear discharge. The distance between the electrodes of the low-voltage plasma generator ranges from 3.5 to 9.5 mm. The plasma discharge is produced by using the low-voltage actuator embedded in the projectile.

D. Free Pitching Projectile Motion Device

Another series of experiments is conducted with a projectile model mounted on a sting ending with an axis in such a way that the model can turn around that pitching axis exactly located at the center of gravity of the model. The aim of the experimental study consists of recording the free pitching motion of the projectile using a high-speed camera. The analysis of the recorded images allows the determination of the pitching response of the projectile model as far as the evolution of the measured angle of attack is concerned.

The main difficulty encountered in that study concerns the projectile-model stability. Figure 5 shows the free pitching projectile motion device supporting a model (part 1) with an angle of attack. Before the beginning of the experiment, the model is horizontal and locked by a pneumatic jack (parts 2 and 3) and remains locked until the steadiness of the supersonic flow is reached (about 10 s). Then the pneumatic jack fixed to the wind-tunnel support (part 4) releases the model; it is now able to rotate freely around its center of gravity. If the projectile model remains horizontal, the projectile model is stable in the flow; otherwise, it rotates until the angular stop is reached, as shown in Fig. 5. The maximum amplitude of the projectile-model deviation is ± 2.5 deg.

Three projectile models have been tested; they have the same geometry except for the fin height L, which is $0.5D$, D, and $1.5D$, respectively (Fig. 6). The diameter D of the cylindrical part is 20 mm, and it is the reference dimension. The models are made of many parts so that the center of gravity is located at the pitching axis, as mentioned earlier. The electrodes flush with the conical surface are situated at the model tip or just in front of the cone–cylinder junction. The plasma discharge produced by using the low-voltage actuator is located outside the wind tunnel due to the dimensions of the actuator and projectile models.

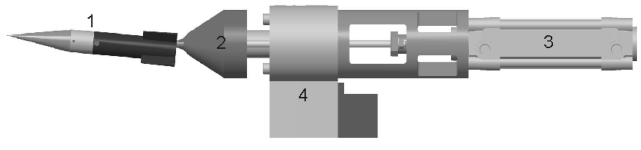

Fig. 5 Projectile model mounted on the free pitching motion device.

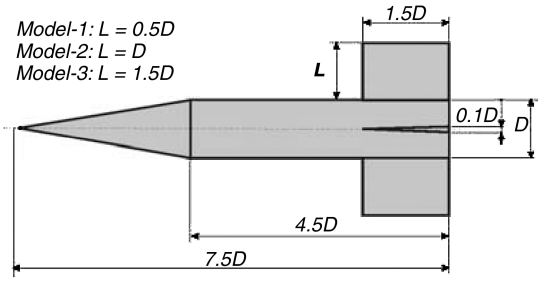

Fig. 6 Projectile-model geometries for the free pitching motion study.

E. Measurements and Visualizations

The measurements of the voltage and current during the plasma discharge are recorded. The voltage measurement made at the electrode bounds indicates the lifetime of the plasma discharge. The current measurement gives a representation of the impulsiveness of the plasma discharge.

The plasma discharge is produced at the projectile nose when the flow is quasi steady around the model. A DI system or a schlieren method is used for visualizing the flowfield structure by means of a charge-coupled device (CCD) camera. The DI works as a flow visualization technique [59] based on the density-gradient field, thus allowing the gathering of information on an interferogram showing the flow pattern around the model. The DI apparatus is set for a gas at rest so as to obtain fringe patterns or an infinite fringe width showing a homogeneous light intensity distribution. In the present experiments the DI apparatus is used following the second adjustment and the pictures look like schlieren pictures. In this way, the density-gradient field in the gas flow is visualized in terms of the light intensity distribution shown on the interferogram pictures. The DI is adjusted in such a way that the density-gradient direction is vertical.

V. Results

A. Wind-Tunnel Facility, $M = 3$, Fixed-Model Device

Many experiments have been carried out with the low-voltage actuator embedded in the 50-mm-diam model for different electrode distances, capacitors, and supplying voltages. The current study has focused only on the first 60 mm of the conical nose to highlight the evolution of the plasma discharge in detail.

The DI pictures (interferograms) are recorded by a 12-bit PCO SENSICAM camera with a spatial resolution of 1280× 1024 pixels^2 and an exposure time of 0.2 μs. The plasma discharge is produced under wind-tunnel conditions at $M = 3$ without any angle of attack. The electrode distance is 3.5 mm.

A first series of interferograms is taken for a configuration in which the energy (E) stored in the capacitor amounts to 12 J. Figure 7 shows shots taken at three instants after the beginning of the plasma discharge to analyze the evolution of the modified flowfield by the plasma. The formation and growth of the disturbance and its propagation along the model conical surface are clearly highlighted. At $t = 17$ μs, the plasma produces an expansion of the air leading to the distortion of the attached shock wave present at the conical tip. The boundary layer is also perturbed by the plasma, but the flowfield modification is larger on the plasma side than on the opposite side. At $t = 50$ μs, the plasma power decreases, the bubble due to the sudden expansion is convected along the model surface, and the attached shock wave remains distorted. At $t = 100$ μs, the plasma power slightly decreases as long as the capacitor is able to provide sufficient energy to maintain it. Its extinction occurs after nearly 250 μs.

A second series of interferograms is taken for $E = 50$ J. Figure 8 shows pictures taken at the same instants so that the influence of the energy delivered to the plasma discharge can be analyzed; a saturation of some CCD pixels is visible for the first instant due to the relatively high exposure time. The effects of the plasma are much greater when the energy is increased and the plasma-discharge duration is longer. Indeed, its extinction takes place after nearly 400 μs.

The visualizations show that the generation of a plasma discharge causes a perturbation between the projectile surface and the shock wave attached to the conical projectile tip. The perturbation is much larger than the one obtained with the high-voltage generator depicted in Fig. 2. It is maintained for a certain length of time and is strong enough to distort the attached shock wave: the higher the energy, the stronger the perturbation and the longer the plasma-discharge duration. The perturbation is more important on the plasma-discharge side than on the opposite side of the projectile tip, leading to an imbalance in the flowfield.

The influence of the energy is clearly examined by using capacitors capable of supplying 7, 12, and 50 J. Figure 9 shows interferograms taken 50 μs after the beginning of the plasma

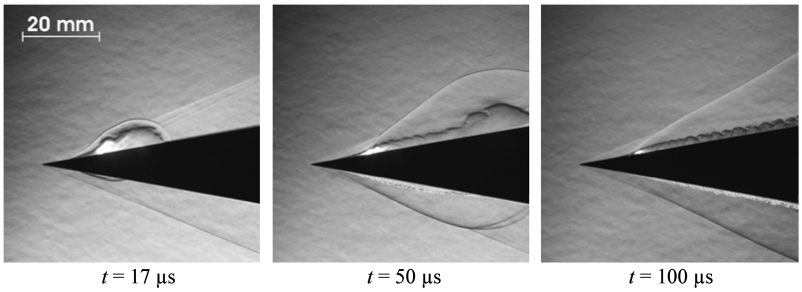

$t = 17$ μs $t = 50$ μs $t = 100$ μs

Fig. 7 Plasma-discharge visualizations at $M = 3$, $E = 12$ J, time evolution.

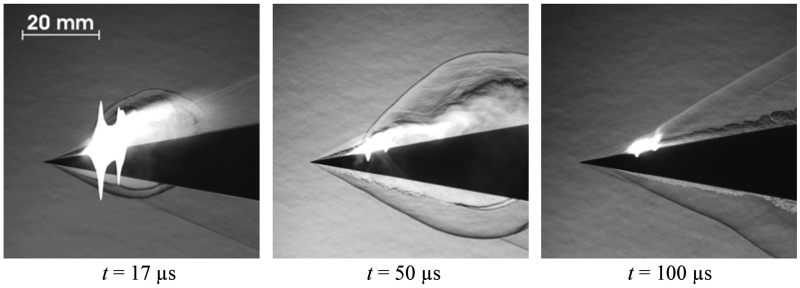

$t = 17$ μs $t = 50$ μs $t = 100$ μs

Fig. 8 Plasma-discharge visualizations at $M = 3$, $E = 50$ J, time evolution.

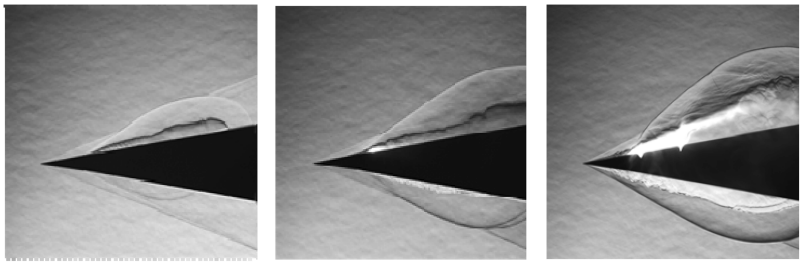

$E = 7$ J $E = 12$ J $E = 50$ J

Fig. 9 Plasma-discharge visualizations at $M = 3$, $t = 50$ μs, energy influence.

discharge for an electrode distance of 9.5 mm: the higher the supplied energy, the larger the perturbation. The analysis of these flowfield structures must be considered very carefully; the fact that the perturbation is greater when the highest energy is used does not mean that the pressure imbalance on the projectile surface is stronger.

The influence of the electrode distance is examined by performing other series of interferograms taken for four electrode distances (l) and $E = 50$ J. Figure 10 shows interferograms taken 50 μs after the beginning of the plasma discharge.

The sparks indicating the electrode pairs of the low-voltage plasma generator are visible on each interferogram. There are small differences in the flow structures just after the beginning of the process, which means that the delivered power is nearly the same. However, the plasma duration depends on the electrode distance, as can be seen in Fig. 11.

Figure 11 represents the voltage evolution measured between the electrodes of the low-voltage plasma generator during the earlier experiments. Before the plasma discharge occurs at $t = 0$, the voltage between the electrodes is 558 V, corresponding to the capacitor voltage. The plasma-discharge start produces a voltage drop down to about 220 V, depending on the electrode distance, as the same capacitor is used. The voltage slightly decreases and the plasma extinction takes place when a slight voltage increase occurs up to a residual value. The plasma duration increases from 0.34 ms for tip 4 to 0.42 ms for tip 1 as the electrode distance decreases; indeed, the longer the electrode distance, the higher the voltage necessary to keep the discharge active.

B. Wind-Tunnel Facility, $M = 3$, Free Pitching Projectile Motion Device

The models defined in Sec. IV.D. (Fig. 6) have been tested without any plasma discharge as a first step. As mentioned in that section, at the beginning of the experiment the projectile model is horizontal and remains locked until the steadiness of the supersonic flow is reached. The model is then unlocked and is able to rotate freely around its pitching axis, which is also its center of gravity. On the one hand, model 1 is unstable; on the other hand, models 2 and 3 are stable, which means that the projectile model remains horizontal. About 20 series of experiments are conducted with model 2 to examine the behavior of the projectile model submitted to a plasma discharge.

Four series of tests are analyzed in this section in terms of flowfield visualizations, projectile-tip displacement corresponding to the angle-of-attack deviation, and voltage-current evolution. The plasma discharge is generated at the tip (electrode distance of 9.5 mm) and at the cone–cylinder junction (electrode distance of 3.5 mm) of the projectile model. The low-voltage actuator is located outside the wind tunnel. Two values of the capacitor are considered, and a coil is added to the low-voltage actuator to increase the plasma duration.

1. *Discharge at the Model Tip; $E = 33.4$ J*

The plasma discharge is produced at the tip of the projectile model in the same way as for the earlier tests. Schlieren pictures are recorded by a Photron Fastcam camera at 6000 frames per second with a spatial resolution of 640×240 pixels^2 and an exposure time of 1 μs. Figure 12a presents the schlieren picture of the flowfield around the projectile model without any discharge. Behind the projectile fins, the mobile part (part 2 in Fig. 5) driven by the pneumatic jack (part 3) is removed from the projectile model; the projectile model is perfectly stable and the symmetrical nature of the flow is well highlighted. In Fig. 12b, a plasma discharge is generated and the perturbation is visualized about 100 μs after its occurrence. The plasma discharge disturbs the flowfield more on the upper side than on the lower side of the projectile.

2. *Discharge in Front of the Cone–Cylinder Junction of the Model; $E = 33.4$ J*

The plasma discharge is generated in front of the cone–cylinder junction (or shoulder) of the projectile model, that is, just in front of the expansion wave. The visualization is performed identically to the previous one. Figures 13a and 13b show the flowfield around the

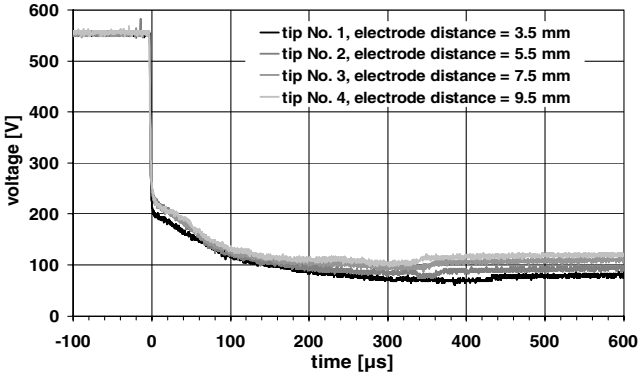

Fig. 11 Voltage measurement during the plasma discharge with four electrode distances.

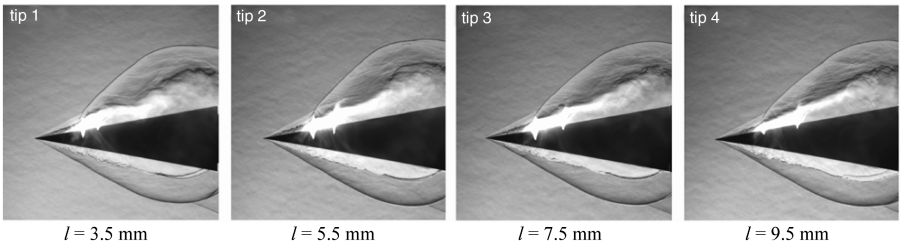

$l = 3.5$ mm $l = 5.5$ mm $l = 7.5$ mm $l = 9.5$ mm

Fig. 10 Plasma-discharge visualizations at $M = 3$, $t = 50$ μs, $E = 50$ J, electrode-distance influence.

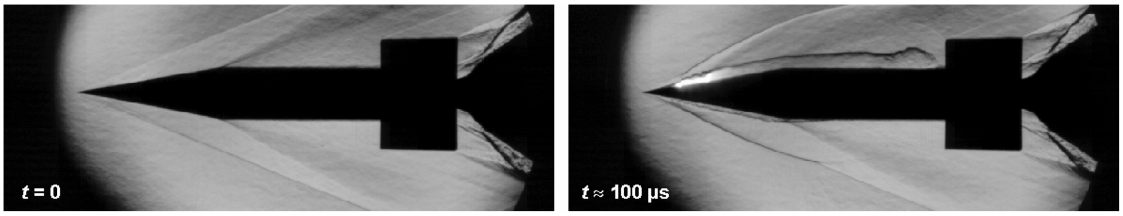

Fig. 12 Free pitching projectile evolution during the plasma discharge at the model tip, $M = 3$, $E = 33.4$ J (test 08-01-14-02).

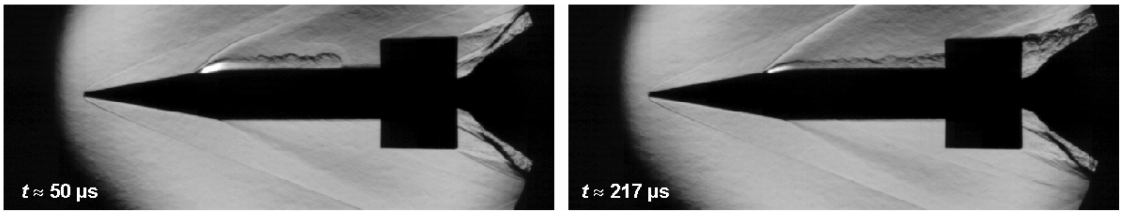

Fig. 13 Free pitching projectile evolution during the plasma discharge at the cone–cylinder junction, $M = 3$, $E = 33.4$ J (test 08-01-14-01).

projectile model disturbed by the plasma discharge; the perturbation is visualized about 50 and 217 μs, respectively, after its production. The plasma discharge disturbs the flowfield only on the upper side and interacts with the fins.

The evolution of the voltage and current measured during the plasma discharge is shown in Fig. 14 for these tests. The plasma discharge ends when the current reaches zero; thus, the plasma is maintained for about 0.75 ms. The curve shapes are similar for both tests, but there are differences in amplitude because the electrode distances are not identical: the longer the electrode distance, the lower the current and the higher the remaining voltage. The maximum current is of the order of 600 and 700 A in the case of a plasma discharge generated at the tip and on the shoulder of the projectile model, respectively.

The analysis of the videos of these two tests allows the determination of the projectile-tip trajectory; thus, the angular deviation of the projectile model can be measured. The angle-of-attack evaluation is performed by using an intercorrelation method of two successive images of the projectile tip. A subpixel method with an accuracy of 0.1 pixel allows the detection of the intercorrelation peak on the images. Taking into account the optical calibration system, the accuracy of the displacement measurement is 34 μm/pixel, leading to an angle-measurement uncertainty of 10^{-5} deg.

Figure 15 presents that angular deviation as a function of time. The discharge current shown in Fig. 14 is plotted again in Fig. 15 so that the current can be correlated with the angular deviation. The instant of the plasma-discharge production is the reference time of the graph. Before the plasma discharge is activated, the projectile model makes a slight pitching motion of about ± 0.20 deg of amplitude and its motion period is of 19.722 ms, corresponding to its natural pitching frequency of 50.7 Hz. The plasma-discharge activation causes an inversion of the projectile-model deviation followed by a very slight amplification of the motion.

3. Discharge at the Model Tip; $E = 243$ J

The plasma discharge is generated at the tip of the projectile model in the same way as for the first test series, but the stored energy is about 7 times higher. Schlieren pictures are recorded at 18,000 frames per second, and the spatial resolution and the exposure time remain the same. Six pictures are extracted from the video, and they clearly show the perturbation evolution (Fig. 16). The flowfield is obviously more disturbed than in the first test series.

4. Discharge in Front of the Cone–Cylinder Junction of the Model; $E = 243$ J

The plasma discharge occurs in front of the cone–cylinder junction of the projectile model. The visualization is performed identically to the previous one. Figure 17 presents six pictures extracted from the video showing the flowfield around the projectile model disturbed by the plasma discharge, which perturbs the flowfield mainly on the upper side and leads to a large imbalance of the density field. The comparison of that figure with the previous one emphasizes the differences in the flowfield for the two configurations.

The evolution of the voltage and the current measured during the plasma discharge is shown in Fig. 18 for these tests. The plasma discharge is maintained for about 2.5 ms. Again the curve shapes are similar, but there are differences in amplitude for the same reasons as

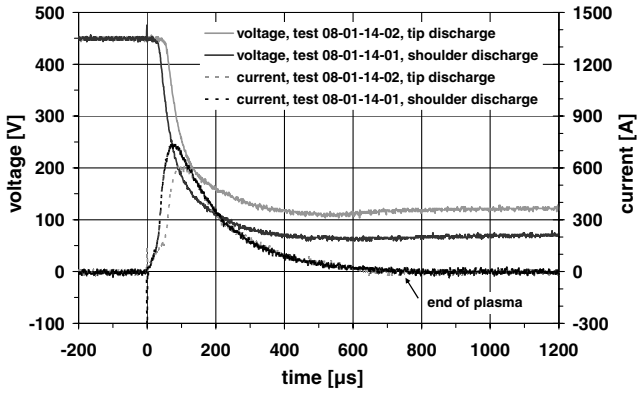

Fig. 14 Voltage and current measured during the plasma discharge, $M = 3$, $E = 33.4$ J.

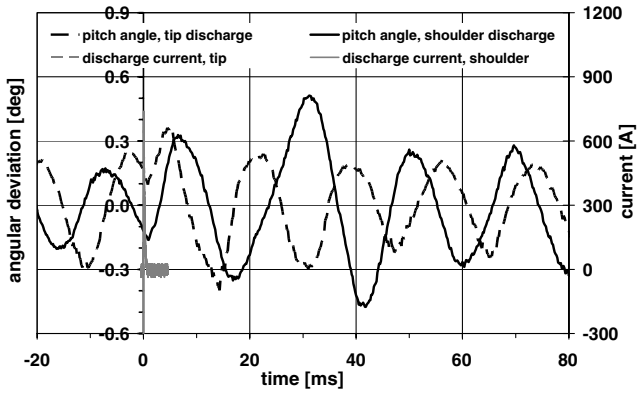

Fig. 15 Angular deviation of the projectile model submitted to the plasma discharge, $M = 3$, $E = 33.4$ J.

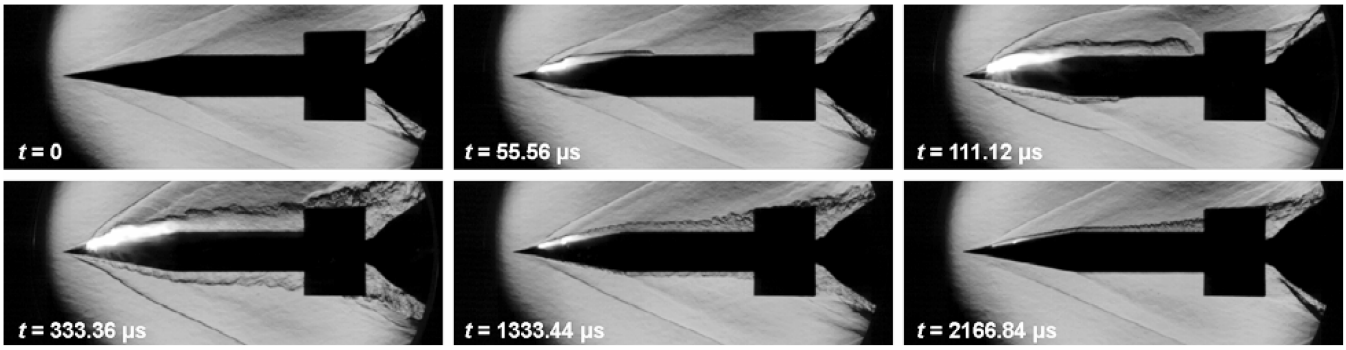

Fig. 16 Free pitching projectile evolution during the plasma discharge at the model tip, $M = 3$, $E = 243$ J (test 08-01-14-06).

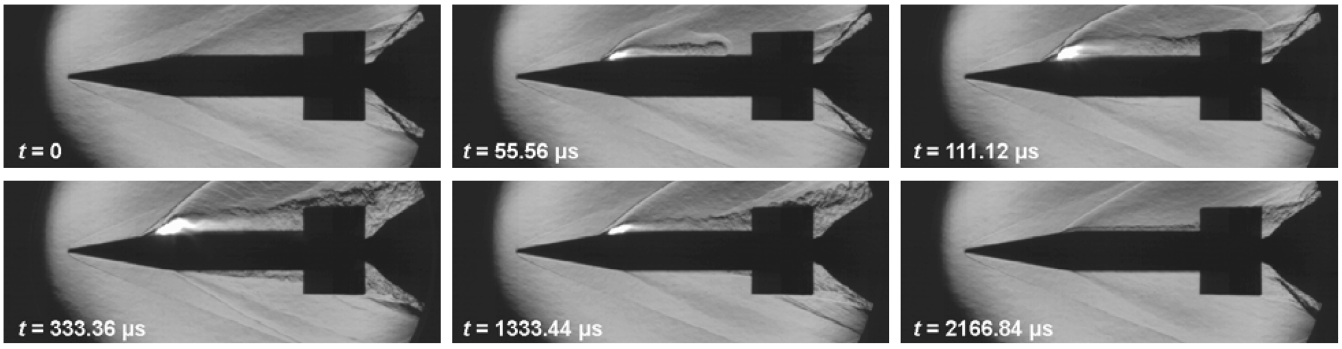

Fig. 17 Free pitching projectile evolution during the plasma discharge at the cone–cylinder junction, $M = 3$, $E = 243$ J (test 08-01-11-01).

those mentioned in reference to Fig. 14. The maximum current is of the order of 1000 and 1300 A when the plasma discharge is generated at the tip and on the shoulder, respectively.

Figure 19 presents the angular deviation as a function of time determined from the analysis of the videos of these two tests. It must be kept in mind that the highest and the lowest possible angles are of ± 2.5 deg. The discharge current is also plotted. The instant of the plasma-discharge production is the reference time of the graph. As in Fig. 15, the projectile model makes a slight pitching motion of about ± 0.15 deg of amplitude before the plasma discharge is activated, corresponding to its natural pitching frequency of 50.7 Hz. There is a delay of about 2 ms between the plasma-discharge generation and the deviation of the projectile model. The maximum amplitudes are observed 8.83 and 7.17 ms after the discharge occurrence and are of 2 and 1.5 deg when the discharge takes place on the shoulder and at the tip, respectively. After the maximum amplitudes have been reached, the projectile model makes a damped pitching motion.

For the same plasma-discharge energy and duration, the projectile deviation is greater for the discharge produced on the shoulder than for the one generated at the tip. That result can be analyzed as follows. The schlieren pictures in Fig. 16 show that, in spite of a density-gradient imbalance, the perturbation caused by the plasma discharge completely surrounds the projectile model when the power is delivered at the projectile-model tip. This is particularly visible on pictures between $t = 111.12$ and 333.36 μs, when the delivered power is maximum (Fig. 18). In Fig. 17 it can be seen that the perturbation also surrounds the projectile near $t = 333.36$ μs, when the power is delivered at the projectile-model shoulder, but less than when power is delivered to the tip. Consequently, the density-gradient imbalance is greater when the power is delivered at the shoulder than at the tip, leading to a better efficiency when the plasma discharge is generated near the shoulder than near the tip.

The results show a significant change in the angle of attack of the projectile 2.5 ms after the plasma-discharge generation of 243 J. However, the experiments cannot demonstrate that such a plasma discharge induces a change in the trajectory of the projectile, because it is fixed at its gravity center. The remaining questions are "Does this disturbance last long enough to cause the trajectory of the projectile to change?" and "Is the power high enough for a change in the trajectory of the projectile to take place?" Some experiments in

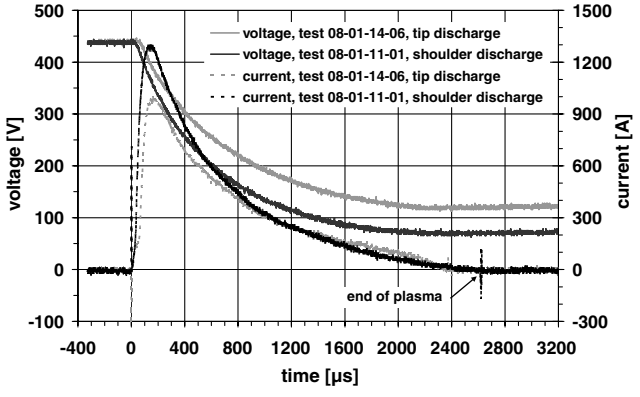

Fig. 18 Voltage and current measured during the plasma discharge, $M = 3$, $E = 243$ J.

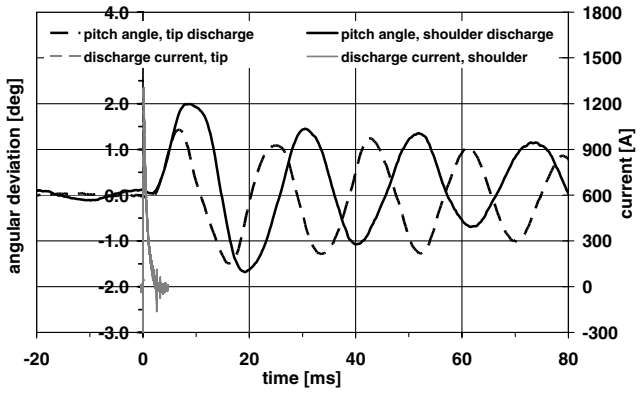

Fig. 19 Angular deviation of the projectile model submitted to the plasma discharge, $M = 3$, $E = 243$ J.

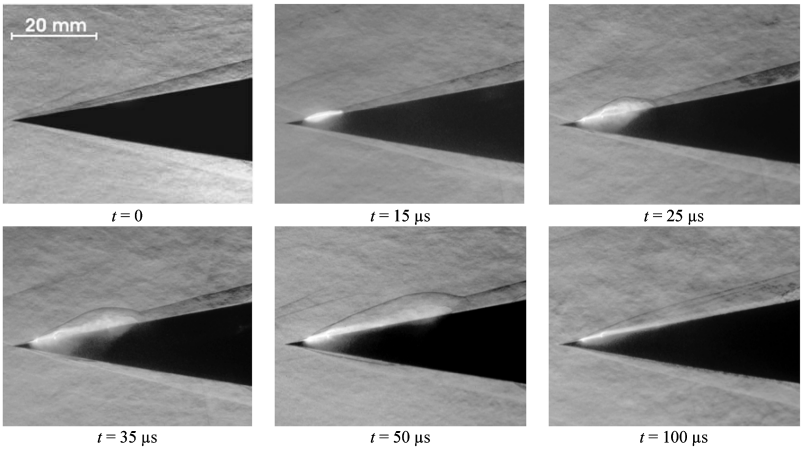

Fig. 20 Plasma-discharge visualizations at $M = 6$, 15 km altitude, $E = 50$ J, time evolution.

the wind tunnel are being continued along these lines to increase the plasma-discharge lifetime, keeping the angle of attack for a longer time; the use of a current regulator allows a better temporal distribution of the power during the plasma discharge. Soon, the trajectory change will be computed by running a 3-DOF program that will use data extracted from these experimental results. Other studies have already been started in the shock-tube facility, in which a projectile can fly freely for some milliseconds and its behavior can be analyzed.

C. Shock-Tube Facility: Projectile at an Altitude of 15 km, $M = 6$, Fixed-Model Device

More experiments have been carried out in the shock-tunnel facility to prove the feasibility of activating a plasma discharge at the tip of a supersonic projectile flying in real conditions. Plasma discharges have been generated on the fixed model at $M = 6$ and an altitude of 15 km. Series of interferograms have been taken with a PCO hsfc pro camera for an exposure time of 0.1 μs.

Figure 20 shows pictures taken before the plasma discharge ($t = 0$) and at five instants after the start of the plasma discharge. The energy stored in the capacitor amounts to 50 J. The electrode distance is 9.5 mm. The visualizations prove again that the generation of a plasma discharge causes a perturbation between the projectile surface and the shock wave attached to the conical projectile tip. Because of the short exposure time, small structures are visible in addition to the main structures of the flow.

VI. Conclusions

The ISL wind-tunnel and shock-tube facilities have been used for visualizing in detail the interaction of a plasma discharge generated at the tip of a conical projectile with a crossflow at supersonic speeds by using a low-voltage plasma actuator embedded in a 50-mm-caliber projectile model. This low-voltage plasma-actuator has been developed with the aim of producing a plasma discharge anywhere on the surface of a supersonic or hypersonic projectile.

Flowfield visualizations have been carried out in the wind tunnel at a Mach number of 3 and obtained by means of a CCD camera located behind a differential interferometer or a schlieren method. These visualizations have allowed the analysis of the perturbation evolution along the projectile surface due to the plasma discharge. The wind tunnel has also been used for demonstrating that the plasma discharge generates the angular deviation of a 20-mm-caliber fin-stabilized projectile, but the low-voltage plasma actuator is outside the model. The density-gradient imbalance is greater when the power is delivered at the cone–cylinder junction than at the tip of the projectile model, leading to a better efficiency when the plasma discharge is generated near the shoulder than near the tip. An angle of attack of 2 deg has been reached by means of a plasma discharge with 243 J of stored energy delivered in 2.5 ms at the cone–cylinder junction of the projectile.

The shock tube serving as a wind tunnel is a facility well adapted to the experimental study of the steering of a supersonic projectile flying under low-atmosphere conditions. The flowfield visualizations prove that a plasma discharge can be produced at the tip of a projectile flying at an altitude of 15 km and a Mach number of 6.

In short, on the one hand, a low-voltage plasma actuator is embedded in a 50-mm-caliber projectile model. On the other hand, the angular deviation is demonstrated with a 20-mm-caliber fin-stabilized projectile with a low-voltage plasma actuator mounted outside the wind tunnel. As a consequence, the final plasma-actuator device could be realized in a caliber ranging from 20 to 50 millimeters, but the plasma actuator needs to be optimized to control the temporal power distribution and miniaturized.

The studies will continue in wind-tunnel and shock-tube facilities with the aim of increasing the angular deviation of the projectile and of evaluating the trajectory deviation. Some experiments will go on in the wind tunnel to increase the plasma-discharge lifetime, keeping the angle of attack for a longer time; a better temporal distribution of the power during the plasma discharge will be achieved by using a current regulator. Soon, the trajectory change will be computed by running a 3-DOF program using data extracted from these experimental results. Other experiments will be conducted in the shock-tube facility, in which a projectile can fly freely for some milliseconds and its behavior analyzed in terms of projectile deviation.

The electrodes of such a type of plasma actuator can be mounted anywhere on the projectile surface or embedded in other parts of it, especially in fins and canards. This concept can also be applied to other sub-, super-, or hypersonic flying vehicles such as missiles, unmanned aerial vehicles, micro air vehicles, and waveriders, among others. However, an optimization phase is necessary for each application and this is long-term work. This is due to the fact that the resulting aerodynamic forces and moments depend on such factors as the Mach number, angle of attack, number of actuators, delivered energy and voltage, actuator location, electrode distance.

Acknowledgment

The authors thank the Aerodynamics and Wind-Tunnel Department and the Aerothermodynamics and Shock-Tube Department staff members of the French–German Research Institute of Saint-Louis for their efficiency.

References

[1] Berner, C., and Dupuis, A., "Wind Tunnel Tests of a Grid Finned Projectile Configuration," AIAA Paper 2001-0105, Jan. 2001.

[2] Dupuis, A., and Berner, C., "Aerodynamic Aspects of a Grid Finned Projectile at Subsonic and Supersonic Velocities," *19th International*

Symposium on Ballistics, Defense Technical Information Center , Fort Belvoir, VA, May 2001.
[3] Berner, C., and Dupuis, A., "Wind Tunnel Tests of a Long-Range Artillery Shell Concept," AIAA Paper 2002-4416, Aug. 2002.
[4] Berner, C., Fleck, V., and Dupuis, A., "Experimental and Computational Analysis for a Long-Range Spinning Artillery Shell with Lifting Surfaces," *20th International Symposium on Ballistics*, Defense Technical Information Center , Fort Belvoir, VA, Sept. 2002.
[5] Dupuis, A., Berner, C., and Fleck, V., "Aerodynamic Characteristics of a Long-Range Spinning Artillery Shell. Part 1: From Aeroballistic Range Free-Flight Tests," *21st International Symposium on Ballistics*, Defense Technical Information Center , Fort Belvoir, VA, April 2004.
[6] Srulijes, J., Seiler, F., Hennig, P., and Gleich, P., "Visualisierung der Umströmung von Lenkflügeln im Stoßrohr-Windkanal bei Realen Atmosphärischen Strömungsbedingungen," French–German Research Institute of Saint-Louis Rept. RV 229/2004, 2004.
[7] Patel, M. P., Prince, T. S., Carver, R., DiCocco, J. M., Lisy, F. J., and Ng, T. T., "Deployable Flow Effectors for Phantom Yaw Control of Missiles at High Alpha," AIAA Paper 2002-2827, June 2002.
[8] Silton, S. I., "Comparison of Predicted Actuator Performance for Guidance of Supersonic Projectiles to Measured Range Data," AIAA Paper 2004-5195, Aug. 2004.
[9] Massey, K. C., McMichael, J., Warnock, T., and Hay, F., "Design and Wind Tunnel Testing of Guidance Pins for Supersonic Projectiles," Georgia Inst. of Technology, Atlanta, GA, Dec. 2004.
[10] Gnemmi, P., and Seiler, F., "Interaction of a Lateral Jet with the Projectile External Flow," AIAA Paper 2000-4196, Aug. 2000.
[11] Schäfer, H. J., Augenstein, E., Esch, H., and Emunds, H., "Experimental Investigation of Transverse Jet Interaction on a Missile Body Using Laser Velocimetry and Flow Visualization," *19th International Congress on Instrumentation in Aerospace Simulation Facilities*, IEEE Xplore Digital Library, Aug. 2001.
[12] Seiler, F., Gnemmi, P., Ende, H., Schwenzer, M., and Meuer, R., "Jet Interaction at Supersonic Cross-Flow Conditions," *Shock Waves*, Vol. 13, No. 1, July 2003, pp. 13–23. doi:10.1007/s00193-003-0189-y
[13] Gnemmi, P., and Schäfer, H. J., "Experimental and Numerical Investigations of a Transverse Jet Interaction on a Missile Body," AIAA Paper 2005-0052, Jan. 2005.
[14] Havermann, M., Seiler, F., Ende, H., and George, A., "Untersuchungen im Stossrohr-Windkanal zur Steuerung eines Hochgeschwindigkeits-Flugkörpers mit Seitenstrahlen," French–German Research Institute of Saint-Louis Rept. RV 232/2004, 2004.
[15] Yamanaka, T., and Tanaka, H., "Effects of Impulsive Thruster on Exterior Ballistics Accuracy Improvement for a Hypervelocity Rocket," *16th International Symposium on Ballistics*, Defense Technical Information Center , Fort Belvoir, VA, Sept. 1996.
[16] Wey, P., Berner, C., Sommer, E., Fleck, V., and Moulard, H., "Theoretical Design for a Guided Supersonic Projectile," *22nd International Symposium on Ballistics*, Defense Technical Information Center , Fort Belvoir, VA, 2005.
[17] Gnemmi, P., Samirant, M., and Charon, R., French–German Research Institute of Saint-Louis, Saint-Louis Cedex, France, French Patent for "Pilotage d'un Projectile par Décharge Plasma," No. 02 12906 filed 17 Oct. 2002, issued 7 Jan. 2005; also US Patent for "Projectile Steering by Plasma Discharge," No. US 7,002,126 B2 filed 17 Oct. 2003, issued 21 Feb. 2006.
[18] Gnemmi, P., and Rey, C., French–German Research Institute of Saint-Louis, Saint-Louis Cedex, France, French Patent for "Nouveau Dispositif Embarqué de Génération de Décharge(s) Plasma pour le Pilotage d'un Engin Supersonique ou Hypersonique," No. 05 09831 filed 27 Sept. 2005, issued 14 Dec. 2007; also US Patent for "Low Voltage Device for the Generation of Plasma Discharge to Operate a Supersonic or Hypersonic Apparatus," No. US 11/525,169 filed 22 Sept. 2006, published 30 Aug. 2007.
[19] Corke, T. C., Post, M. L., and Orlov, D. M., "Single Dielectric Barrier Discharge Plasma Enhanced Aerodynamics: Physics, Modelling and Applications," *Experiments in Fluids*, Vol. 46, 2009, pp. 1–26. doi:10.1007/s00348-008-0582-5
[20] Kuo, S. P., "Plasma Mitigation of Shock Wave: Experiments and Theory," *Shock Waves*, Vol. 17, 2007, pp. 225–239. doi:10.1007/s00193-007-0112-z
[21] Elias, P. Q., Chanetz, B., Larigaldie, S., and Packan, D., "Study of the Effect of Glow Discharges Near a $M = 3$ Bow Shock," *AIAA Journal*, Vol. 45, No. 9, Sept. 2007, pp. 2237–2245. doi:10.2514/1.28515
[22] Shneider, M. N., Macheret, S. O., Zaidi, S. H., Girgis, I. G., and Miles, R. B., "Virtual Shapes in Supersonic Flow Control with Energy Addition," *Journal of Propulsion and Power*, Vol. 24, No. 5, Sept.–Oct. 2008, pp. 900–915. doi:10.2514/1.34136
[23] Girgis, I. G., Shneider, M. N., Macheret, S. O., Brown, R. B., and Miles, R. B., "Steering Moments Creation in Supersonic Flow by Off-Axis Plasma Heat Addition," *Journal of Spacecraft and Rockets*, Vol. 43, No. 3, May–June 2006, pp. 607–613. doi:10.2514/1.16708
[24] Kosinov, A., Maslov, A., and Shevelkov, S., "Experiments on the Stability of Supersonic Laminar Boundary Layers," *Journal of Fluid Mechanics*, Vol. 219, 1990, pp. 621–633. doi:10.1017/S0022112090003111
[25] Corke, T. C., Cavalieri, D., and Matlis, E. H., "Boundary Layer Instability on a Sharp Cone at Mach 3.5 with Controlled Input," *AIAA Journal*, Vol. 40, No. 5, 2002, pp. 1015–1018. doi:10.2514/2.1744
[26] Matlis, E. H., "Controlled Experiments on Instabilities and Transition to Turbulence on a Sharp Cone at Mach 3.5.," Ph.D. Dissertation, Univ. of Notre Dame, Notre Dame, IN, 2004.
[27] Elias, P. Q., Chanetz, B., Larigaldie, S., Packan, D., and Laux, C. O., "Mach 3 Shock Wave Unsteadiness Alleviation Using a Negative Corona Discharge," *AIAA Journal*, Vol. 46, No. 8, 2008, pp. 2042–2049. doi:10.2514/1.34674
[28] Corke, T. C., Mertz, B., and Patel, M. P., "Plasma Flow Control Optimized Airfoil," AIAA Paper 2006-1208, 2006.
[29] Nelson, C., Cain, A., Patel, M., and Corke, T. C., "Simulation of Plasma Actuators Using the Wind-US Code," AIAA Paper 2006-634, 2006.
[30] Patel, M. P., Sowle, Z. H., Corke, T. C., and He, C., "Autonomous Sensing and Control of Wing Stall Using a Smart Plasma Slat," AIAA Paper 2006-1207, 2006.
[31] Goeksel, B., Rechenberg, I., Greenblatt, D., and Paschereit, C., "Steady and Unsteady Plasma Wall Jets for Separation and Circulation Control," AIAA Paper 2006-3686, 2006.
[32] Huang, J., "Documentation and Control of Flow Separation on a Linear Cascade of Pak-B Blades Using Plasma Actuators," Ph.D. Dissertation, Univ. of Notre Dame, Notre Dame, IN, 2005.
[33] Huang, J., Corke, T. C., and Thomas, F. O., "Plasma Actuators for Separation Control of Low Pressure Turbine Blades," *AIAA Journal*, Vol. 44, No. 1, Jan. 2006, pp. 51–57. doi:10.2514/1.2903
[34] Huang, J., Corke, T. C., and Thomas, F. O., "Unsteady Plasma Actuators for Separation Control of Low-Pressure Turbine Blades," *AIAA Journal*, Vol. 44, No. 7, July 2006, pp. 1477–1483. doi:10.2514/1.19243
[35] Suzen, Y., Huang, G., and Ashpis, D., "Numerical Simulations of Flow Separation Control in Low-Pressure Turbines Using Plasma Actuators," AIAA Paper 2007-937, 2007.
[36] Wall, J.D., Rivir, R., and Franke, M.E., "Effects of Pulsed-D.C. Discharge Plasma Actuators in a Separated Low Pressure Turbine Boundary Layer," AIAA Paper 2007-942, 2007.
[37] Rizzetta, D., and Visbal, M., "Numerical Investigation of Plasma-Based Flow Control for a Transitional Highly-Loaded Low-Pressure Turbine," AIAA Paper 2007-938, 2007.
[38] Douville, T., Stephens, J., Corke, T. C., and Morris, S. C., "Turbine Blade Tip Leakage Flow Control by Partial Squealer Tip and Plasma Actuators," AIAA Paper 2006-20, 2006.
[39] Van Ness, D. K., and Corke, T. C., and Morris, S. C., "Turbine Tip Clearance Flow Control Using Plasma Actuators," AIAA Paper 2006-21, 2006.
[40] Thomas, F. O., Kozlov, A., and Corke, T. C., "Plasma Actuators for Bluff Body Flow Control," AIAA paper 2006-2845, 2006.
[41] Asghar, A., Jumper, E. J., and Corke, T. C., "On the Use of Reynolds Number as the Scaling Parameter for the Performance of Plasma Actuator in a Weakly Compressible Flow," AIAA Paper 2006-170, 2006.
[42] Do, H., Kim, W., Mungal, M., and Capelli, M., "Bluff Body Flow Control Using Surface Dielectric Barrier Discharges," AIAA Paper 2007-939, 2007.
[43] Balcer, B. E., Franke, M. E., and Rivir, R. B., "Effects of Plasma Induced Velocity on Boundary Layer Flow," AIAA Paper 2006-875, 2006.
[44] Porter, C., McLaughlin, T., Enloe, L., and Font, G., "Boundary Layer Control Using DBD Plasma Actuator," AIAA Paper 2007-786, 2007.
[45] Visbal, M. R., and Gaitonde, D. V., "Control of Vortical Flows Using Simulated Plasma Actuators," AIAA Paper 2006-505, 2006.
[46] Nelson, R., Corke, T. C., Patel, M., and Ng, T., "Modification of the Flow Structure Over a UAV Wing for Roll Control," AIAA Paper 2007-884, 2007.
[47] Post, M. L., "Plasma Actuators for Separation Control on Stationary and

Unstationary Airfoils," Ph.D. Dissertation, Univ. of Notre Dame, Notre Dame, IN, 2004.
[48] Post, M. L., and Corke, T. C., "Separation Control Using Plasma Actuators—Stationary and Oscillatory Airfoils," AIAA Paper 2004-841, 2004.
[49] Post, M. L., and Corke, T. C., "Separation Control on High Angle of Attack Airfoil Using Plasma Actuators," *AIAA Journal*, Vol. 42, No. 11, Nov. 2004, pp. 2177–2187. doi:10.2514/1.2929
[50] Corke, T. C., He, C., and Patel, M., "Plasma Flaps and Slats: an Application of Weakly-Ionized Plasma Actuators," AIAA Paper 2004-2127, 2004.
[51] Gnemmi, P., Charon, R., Dupéroux, J. P., and George, A., "Feasibility Study for Steering a Supersonic Projectile by a Plasma Actuator," *AIAA Journal*, Vol. 46, No. 6, 2008, pp. 1308–1317. doi:10.2514/1.24696
[52] Gnemmi, P., and Rey, C., "Guidance of a Supersonic Projectile by a Plasma Actuator," *23rd International Symposium on Ballistics*, Defense Technical Information Center , Fort Belvoir, VA, April 12007.
[53] Raizer, Yu. P., *Gas Discharge Physics*, Springer–Verlag, New York/Berlin/Heidelberg, 1991.
[54] Gnemmi, P., Eichhorn, A., Leopold, F., Schäfer, H. J., Emunds, H., Esch, H., and Gülhan, A., "Experimental and Computational Study of the Interaction between a Lateral Jet and the Supersonic External Flow on a Generic Missile Body," French–German Research Institute of Saint-Louis Rept. PU 622/2006, May 2006.
[55] Patz, G.,"Das Hyperschallstossrohrlabor des ISL, 3. Teil: Stossrohr B," French–German Research Institute of Saint-Louis Rept. N 30/70, Sept. 1970.
[56] Patz, G., "Das Hyperschallstossrohrlabor des ISL, 2. Teil: Stossrohr A," French–German Research Institute of Saint-Louis Rept. N 27/71, Nov. 1971.
[57] Oertel, H., *Stossrohre*, Springer–Verlag, Vienna/New York, 1966.
[58] Seiler, F., Srulijes, J., Havermann, M., Hennig, P., and Gleich, P., "Heat-Transfer Measurements at the Nose of a High-Speed Mach 6 Missile," French–German Research Institute of Saint-Louis, Rept. S-PU 616/2006, May 2006.
[59] Smeets, G., "Interferometry," French–German Research Institute of Saint-Louis Rept. CO 214/90, May 1990.

M. Costello
Associate Editor